LCSB-inception: Reliable and effective light-chroma separated branches for Covid-19 detection from chest X-ray images

Chiagoziem C. Ukwuoma [a,*], Zhiguang Qin [a,**], Victor Kwaku Agbesi [b], Chukwuebuka J. Ejiyi [a], Olusola Bamisile [c], Ijeoma A. Chikwendu [d], Bole W Tienin [d], Md Altab Hossin [e]

[a] School of Information and Software Engineering, University of Electronic Science and Technology of China, Sichuan, PR China
[b] School of Computer Science and Engineering, University of Electronic Science and Technology of China, Sichuan, PR China
[c] Sichuan Industrial Internet Intelligent Monitoring and Application Engineering Technology Research Center, Chengdu University of Technology, Chenghua District, Chengdu, Sichuan, PR China
[d] School of Information and Communication Engineering, University of Electronic Science and Technology of China, Sichuan, PR China
[e] School of Innovation and Entrepreneurship, Chengdu University, No. 2025, Chengluo Avenue, 610106, Chengdu, Sichuan, PR China

A B S T R A C T

According to the World Health Organization, an estimate of more than five million infections and 355,000 deaths have been recorded worldwide since the emergence of the coronavirus disease (COVID-19). Various researchers have developed interesting and effective deep learning frameworks to tackle this disease. However, poor feature extraction from the Chest X-ray images and the high computational cost of the available models impose difficulties to an accurate and fast Covid-19 detection framework. Thus, the major purpose of this study is to offer an accurate and efficient approach for extracting COVID-19 features from chest X-rays that is also less computationally expensive than earlier research. To achieve the specified goal, we explored the Inception V3 deep artificial neural network. This study proposed LCSB-Inception; a two-path (L and AB channel) Inception V3 network along the first three convolutional layers. The RGB input image is first transformed to CIE LAB coordinates (L channel which is aimed at learning the textural and edge features of the Chest X-Ray and AB channel which is aimed at learning the color variations of the Chest X-ray images). The L achromatic channel and the AB channels filters are set to 50%L-50%AB. This method saves between one-third and one-half of the parameters in the divided branches. We further introduced a global second-order pooling at the last two convolutional blocks for more robust image feature extraction against the conventional max-pooling. The detection accuracy of the LCSB-Inception is further improved by employing the Contrast Limited Adaptive Histogram Equalization (CLAHE) image enhancement technique on the input image before feeding them to the network. The proposed LCSB-Inception network is experimented on using two loss functions (Categorically smooth loss and categorically Cross-entropy) and two learning rates whereas Accuracy, Precision, Sensitivity, Specificity F1-Score, and AUC Score were used for evaluation via the chestX-ray-15k (Data_1) and COVID-19 Radiography dataset (Data_2). The proposed models produced an acceptable outcome with an accuracy of 0.97867 (Data_1) and 0.98199 (Data_2) according to the experimental findings. In terms of COVID-19 identification, the suggested models outperform conventional deep learning models and other state-of-the-art techniques presented in the literature based on the results.

1. Introduction

The well-known coronavirus (COVID-19) has swiftly spread to several countries since its outbreak in Wuhan, China. COVID-19 was first transmitted in an animal-to-human channel [1,2], affecting the respiratory system and several organs including the liver, genitourinary system, and stomach organs. Typically, the Covid-19 symptoms are associated with severe cough, fever, difficulty in breathing, and tiredness, among others. Currently, the virus can migrate to the lower respiratory system and result in pneumonia, a severe form of lung

---

* Corresponding author.
** Corresponding author.
E-mail addresses: ukwuoma@std.uestc.edu.cn (C.C. Ukwuoma), qinzg@uestc.edu.cn (Z. Qin).

inflammation. This type of virus often comes with cytokine release syndrome, which leads to the failure of many organs and the development of acute respiratory distress syndrome (ARDS), leading to death [3, 4]. Three (3) years after the virus has been declared a pandemic by the World Health Organization (WHO) [5], more than 300 million cases have been recorded worldwide and its mortality rate continues to increase daily. Therefore, to reduce the transmission of the novel virus, medical professionals have devised key preventative measures such as distancing from one another, obligatory face mask use, frequent hand washing and sanitizing with alcohol-based hand sanitizers, and, if required, quarantine [6]. Detecting and categorizing COVID-19 is more challenging due to its fast mutation period, dissemination, and appearance of silent infections. Previously, a reverse transcription (RT) - polymerase chain reaction (PCR) and antibody testing methods were used to detect Covid-19 [7]. The RT-PCR-based methods were unable to sustain the high demand for results due to a lack of testing kits, and inaccurate, and divergent results. An antibody test was not a reliable option because it can only be carried out after a certain amount of infection period [8]. Hence, computed tomography (CT) scans [9] and radiographic imaging [10] were chosen over the other imaging techniques for Covid-19 diagnosis. When comparing the radiation emitted by CT and Chest X-ray imaging [11], the Chest X-rays are more secure, less harmful to an individual's health, and efficient and effective in detecting the virus while CT imaging tends to be more harmful to a person's health.

Deep learning (DL) has gained popularity in recent years as a method for autonomously deriving extracted features from raw data. The improvement in processing power over the past few years is mostly to blame for this. Convolutional Neural Networks (CNNs) have been used in various areas of image processing, including segmentation [12] and classification [13]. In medical imaging, feature extraction which is the major drawback of most deep learning networks is caused by the blurriness, occlusion, and illumination variation of the input image [14]. In the area of CNN-based medical image analysis, several works have been put out where the techniques provide effective outcomes. This indicates both the reliability and the widespread use of CNNs [15]. Whenever we have an abundance of things, picking the best or necessary one becomes highly challenging since it takes a long time to search through a large search space. Likewise, how we might not require every feature in a feature set used for classification since there can be several unnecessary features, Due to the enormous number of feature pairings that are conceivable in this situation, selecting the optimum combination of features from the initial feature set can be an extremely costly procedure. The goal of feature selection (FS) is to pick the features that are most pertinent from the available information without sacrificing the learning model's performance.

Following the aforementioned, many strategies have been put forth by various researchers for the identification of Covid-19 in radiological imaging such as CT scans and chest X-rays. In Ref. [16], the authors detected COVID-19 from chest X-rays using the Support Vector Machine (SVM) and the ResNet50 mechanism. They used the ResNet50 as the feature extractor while classifying the extracted feature using the SVM which yielded an accuracy of 95.4%, sensitivity of 97.2% and specificity of 93.4%. Recent pre-trained models have demonstrated an increase in several performance metrics with medical imaging studies. A pre-trained COVID-19 detecting model [17] displayed an overall sensitivity and positive predictive values of 92.9% and 98.9% for COVID-19 pneumonia, 89% and 91.8% for non-COVID-19 pneumonia, and 95% and 88.8% for normal lung tissue. The authors of [18] used transfer DL to categorize X-ray images into pneumonia and healthy chest images with a 96.4% accuracy rate and a 99.62% data recall rate that had never been observed previously. The authors of [19] built a classifier based on CheXNet and transfer learning (TL) to detect: COVID-19, Normal, and Viral Pneumonia X-ray images, which recorded a 97% of accuracy. The primary problem with CNNs' raw characteristics is that some of them could be superfluous or unnecessary. When it comes to the ultimate

prediction exercise, certain elements may be crucial while others may be irrelevant. The number of features and the computation power can both be decreased by removing correlated and redundant information. In rare circumstances, the classification performance may even improve as a result of this. As a result, FS is regarded as a crucial technique for raising the effectiveness of such learning systems, including those that employ DL.

However, Lightweight models with less computational cost and high performance are needed in the medical sector for real-time application. In line with this, dual path CNN has been proposed by researchers for image classification [20,21] which yields better performance with lesser computational cost than the traditional signal path models. Drawing inspiration from Multi-path Convolutional Neural Networks [21] and Dual Paths Neural Networks [26], we developed an Inception V3 [20] based architecture with two paths (branches) along the first three convolutional layers (LCSB-Inception) to identify the texture and patterns of COVID-19-specific X-ray datasets, First, the chest X-ray's RGB images were converted into CIE Lab color coordinates (achromatic L channel and AB channels). The achromatic L channel (aimed at studying the Chest X-ray image textures and edges) is fed into one branch, while the AB channel (aimed at the color variation of the Chest X-ray image) is fed into the other branch. They kept the number of filters equal (50%L −50%AB). The concatenation layer follows the third convolutional layer, after which four other 2D convolutional layers follow. Furthermore, our network replaced the Global average pooling at the end of the network with a Global second-order pooling to exploit more refined image features between the two convolutional networks. The suggested model's performance is further improved by using the CLAHE (Contrast Limited Adaptive Histogram Equalization) Image Quality Enhancement approach on the input image. The main contribution of this paper is as follows;

1. We proposed LCSB-Inception: an inception network-based Dual-Paths light-weight deep Convolutional Neural Network with less memory and computational complexity for fast and accurate Chest X-ray feature extraction for reliable Covid-19 detection.
2. This study introduced the Global second-order pooling at the last two convolutional blocks for comprehensive image information at the last stages of deep ConvNets, in contrast to previous approaches that only employ the max-pooling at the end of the network.
3. We further pre-process the Chest X-ray image data using the CLAHE enhancement technique to generate new deep features and perform a training task with our novel architecture.
4. We reported a well-robust deep learning method in Accuracy, Specificity, Sensitivity, Precision, F1 Score, Confusion matrix, and AUC using receiver operating characteristics (ROC) for detecting Pneumonia and COVID-19, based on the thorough experimental evaluation of the proposed model in comparison with the state-of-the-art results.

This paper is organized into the following sections; The second section is the literature review. The third part outlines the full working methods and material. The dataset details, the evaluation metrics and the experimental setup cover the fourth section while chapter five covers the experimental findings, ablation studies, and result discussions and comparison with the state-of-the-art result. Section 6 is our limitation, conclusion and future works.

2. Related works

Numerous studies have been proposed by both the medical research industry and academia for the classification of COVID-19. This section discusses in depth those related works that gave room for our proposed approach. In light of that, the authors of [23] used a hierarchical analysis to find COVID-19 patterns on CXR images. Several methods were used to generate features out of the images, including Inception-V3 [22].

The authors explore classifiers like SVM, Random Forest, KNNs, MLPs, and Decision Trees for classification. In their results, the COVID-19 class has an F1-Score of 0.89, as stated. Authors in Ref. [24] discovered that COVID-19 CXR sample categorization combining ResNet50 and SVM classifier achieved better accuracy. Other studies have been geared toward automating algorithms to detect CoVID-19, authors in Ref. [25] built an automated DenseNet169 Deep Neural Network (DNN) to detect and diagnose the virus from COVID19 patient's chest samples. Features from these samples were extracted and fed as input tensors to the Extreme Gradient Boosting (XGBoost) mechanism to initiate a classification task in other to determine whether or not a chest image has a trace of COVID-19 based on some preliminaries set previously. They concluded that their proposed model is faster and more precise in detecting the COVID-19 virus from infected chest images.

Deep Learning models require a huge amount of dataset for optimal performance. However, COVID-19 dataset samples are few compared to the traditional ImageNet dataset, hence researchers employed Pre-trained deep learning models via the Transfer learning approach for COVID-19 detection by several researchers. Hemdan et al. [26] evaluated seven (7) popular DL neural network architectures in detecting COVID-19. These models were pre-trained with the ImageNet dataset [27], and only the classifier was trained with radiography. In their analysis, the proposed VGG19 [28] and DenseNET201 [29] performed well. Following a similar strategy [30], the authors presented an extension of the VGG architecture by adding a convolutional COVID block (block). The accuracy reported by the authors for the three-class categorization was 95.3%. In Ref. [31], a novel CNN architecture known as COVID-net was developed to categorize CXR samples into three categories: normal, pneumonia, and COVID-19. According to the authors, COVID-19 had a sensitivity of 80.3% and an overall accuracy of 92.4%. The problem of classifying CXRs samples into normal, COVID-19, bacterial pneumonia, and viral pneumonia is addressed in Ref. [32] fine-tuning with the ResNet50 [33] model. In comparison to the COVID-net, the model was optimized, with an accuracy rate of 96.2% and a sensitivity of 100% for detecting COVID-19. Bekhet et al. [34] surveyed using deep learning techniques and cost-effectiveness evaluation. They went ahead to propose a deep Convolutional Neural Network [35] which yielded an accuracy of 96% for COVID-19 detection as well as efficient lightweight CNN for detecting COVID-19 [36]. Khan et al. [37], present CoroNet, a convolutional neural network-based approach for automating COVID-19 infection diagnosis from chest X-ray images. The proposed model uses the Xception CNN architecture, which has already been trained on the ImageNet dataset. CoroNet was trained and tested on a set of images from two public image databases that were put together as a dataset. The CoroNet model attained an accuracy of 89.6%, with precision and recall rates for COVID-19 cases of 93 and 98.2% for 4-class cases (COVID vs. Pneumonia bacterial vs. Pneumonia viral vs. Normal). Also, the authors test their model on a second dataset, which seems to have the same COVID-19 images that were used for training. Researchers in Ref. [38] compared and analyze the accuracy of InceptionV3, Xception, and ResNeXt models using the 6432 chest X-ray image dataset. The authors asserted that the Xception model had the best accuracy at 97.97%. The study focused on LeakyReLU rather than ReLU as the activation function, suggesting that it is a unique strategy. In conclusion, they observed that there was overfitting during the training phase that lead to the high accuracy. The authors urged further consideration of huge datasets to verify their proposed paradigm.

Despite the proposed approaches, Accurate feature extraction persists yielding to researchers using the ensemble approach. However, the ensemble approach yielded much computational cost of the model which is not accepted in the medical field although the results are much more promising compared to the single models. TL was adopted in a multi-class approach [39], combining VGG19 and MobileNet V2 to classify COVID-19, Pneumonia, and Normal cases. The accuracy index established was far more encouraging than the contemporary studies at

the time. The author of [40] suggests two deep learning frameworks for detecting Covid-19: Deep Hybrid Learning (DHL) and Deep Boosted Hybrid Learning (DBHL). A hybrid model based on CNN and gated recurrent unit (GRU) [41] is proposed to diagnose viral illness from CXRs. In their proposed method, a CNN serves as a feature extraction tool and the GRU was adopted as the classifier. We record that, the model after training with 424 CXR images shows an encouraging effect of 0.96, 0.95, and 0.96 in terms of precision, f1-score, and recall respectively. A novel FB2DEWT (Fixed Boundary-based Two-Dimensional Empirical Wavelet Transform) [42] was used to extract feature modes from the X-ray samples. In their work, a single X-ray sample is decomposed into seven modes and used as an input tensor to the multiscale deep –CNN to classify X-ray samples. Results reveal that the FB2DEWT when applied to X-ray samples from two publicly available datasets with a 5-fold cross-validation technique, achieved maximum accuracy of 96%, 100% and 97.17%, 96.06% for the multiclass and binary classification schemes. This indicates the robustness of FB2DEWT using the public datasets. In their study, G. Bargshady et al. [43] suggested using a learned, semi-supervised CycleGAN in conjunction with GAN algorithm to improve the COVID-19 X-ray and CT Chest Images Dataset. For the experimental trainings, they used a tweaked version of the Inception V3 model via transfer learning and got accuracy of 94.2% and AUC of 92.2%.

To address the issue of Computational complexity, a Covid-19 detecting model based on ConvNet was labeled as "EfficientNet" using CXR images with an accuracy of 93.9%, with 5–30 times fewer parameters recorded with no false prediction [44]. Karakanis et al. [45] suggested two lightweight models, one for binary classification as well as for three-class classification, and compared it to the ResNet8 Pre-trained structure, which is the current state of the art. They attained an accuracy of 96.5% with the suggested binary class model and 94.3% with the multiclass model. The above-mentioned studies so far have a common factor: huge computational complexity and inadequate feature extraction which becomes impractical in real-world implementation, even if the performance accuracy is convincing. Thus, in this study, we presented a well-designed architecture with a remarkable and efficient performance index in identifying covid-19 using a standard Chest X-ray dataset which will be feasible in a real-world implementation. We enhance the original dataset to further get a new dataset with more parameters to train with our novel architecture. This paper is seeking to solve these research gaps with a novel approach for extracting COVID-19 features from chest X-rays that is also less computationally expensive than earlier research.

3. Proposed methodology

This section discusses the proposed architecture and materials in detail. We addressed the two identified research gaps from the related literature which were rich feature extraction and less computational complexity by first splitting the first three convolutional layers of an inceptionV3 variation into two separate branches, secondly, we replaced the Maxpool Layers of the last two convolutional layer with Global second-order pooling [46]. Fig. 1 highlights the flow chart of our model for accurate and enriched feature extraction with less computational cost.

Inception v3 was selected among all known pre-trained models because Toda & Okuras [47] as shown in Fig. 2 have initially reduced the computational complexity of the original inception by getting rid of the last 5 mixed layers out of 11 layers as shown in Fig. 2. However, with a different approach, we further extended their idea by not only reducing the number of the initial convolutions but as well introducing a dual part model with global second-order pooling. Working with a reduced version of Inception V3, this study showed that DCNNs can learn the distinct colors and textures of images like human-made categorization hence we choose that as our baseline.

Having introduced the research gaps and our two-novel approach to
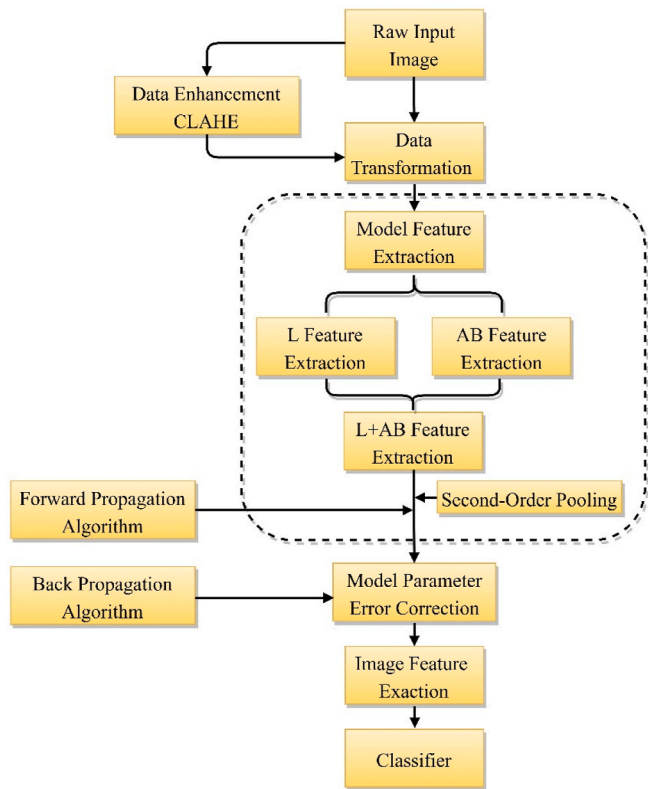
Fig. 1. The proposed model feature extraction flowchart. The raw input image was enhanced using the CLAHE before feeding to the model. The proposed model on the other hand attends to the input by extracting features from two separate channels (L and AB channels) at the first three convolutional layers before concatenating the features. The second-order pooling is further employed for high- and low-level features of the input image.

tackling the identified research gaps, Fig. 3 depicts our proposed model LCSB-Inception. First, the RGB input image is transformed to CIE LAB coordinates where the L channel is been treated separately and the AB channel is treated likewise before the features are joined together. In the sense that shading and shadows produce a variety of RGB values from the inherent color(s) of a surface, we draw our idea from the fact that RGB channels are closely connected [48]. In particular, the three RGB values are modified in the same proportion by intensity fluctuations brought on by changes in light, edges, and texture. Therefore, isolating the L channel's gray-level information and the AB channels' color-related data by converting RGB channels into an achromatic-chromatic space like CIE Lab is effective. From the diagram, the first three layers of the Inception V3 architecture are modified into

two branches to accept the L and AB channels independently. The L channels focused on the textural and edge features of the Chest X-ray images whereas the AB channel focused on the color finding of the Chest X-ray images. we set the filters to 50%L and 50% AB. This approach saves from 1/3 to 1/2 of the parameters in the separated branches. After the L and AB features are treated separately by the first three convolutional layers, the feature is concatenated before we passed the extracted feature to four more convolutional networks. In other to learn higher-order features for improving non-linear modeling capability, we replaced the max-pooling layer of the last two Convolutional layers with a global second-order pooling layer.

The convolution layers used in our proposed model are all 2D convolution and are of the same size (3 x 3) except for the 4th layer (1 x 1). After the Convolutional layers follow a normalization layer before an activation layer. We made use of the ReLU activation function. for the classification head, we passed the Batch normalization layer after a second-order pooling before employing the Dense Layer with Activation GeLu. Another Batch normalization layer is been passed before our last dense layer with the SoftMax activation. Batch Normalization is the layer of a neural network that allows the following layers of the model to adjust more independently [49]. It is used to increase the realism of the preceding layers' output and to scale the activations of the input layer. It may also be used as a regularization to reduce model overfitting. The GeLu activation is the initial Dense layer activation (Gaussian Error Linear Unit). The GeLu was used in this study due to its deterministic nonlinearity, which includes a stochastic regularization effect that results in a large performance boost in most models with intricate topologies [50]. The major role of the SoftMax layer is to turn the encoding Layer's output information into a probability interval (0,1). During training, we used the Adam optimizer, two-loss functions; Categorically smooth loss and categorical cross-entropy loss and two learning rates; 0.001 and 0.0001 to investigate the optimal performance of the model. After reducing the number of convolutional layers while keeping in mind that the main goal of a deep convolutional neural network is to interpret sophisticated boundaries of large numbers of categories in a high-dimensional space, we introduced second-order pooling at the final two convolutional layers because it is essential to learn higher-order features for improving non-linear modeling capability. The employed Second-order pooling is depicted in Fig. 4.

The employed second-order pooling takes a 3D input $h' \times w' \times c'$ where h' denotes heights, w' denotes width and c' denotes channel of the given image, first performs a 1×1 convolution to reduce the channel c' to c since we are most interested in computational complexity reduction. After that follows a pairwise channel connection of $h' \times w' \times c$ that yields to a $c \times c$ variance matrix i.e., the empirical interdependence of channel i with all channels is displayed by the ith row (the polynomial multiplication alters the sequence of the data). A row-wise normalizing on the feature vector is done while keeping the intrinsic compositional information in mind. Before channel scaling, the excitation function uses
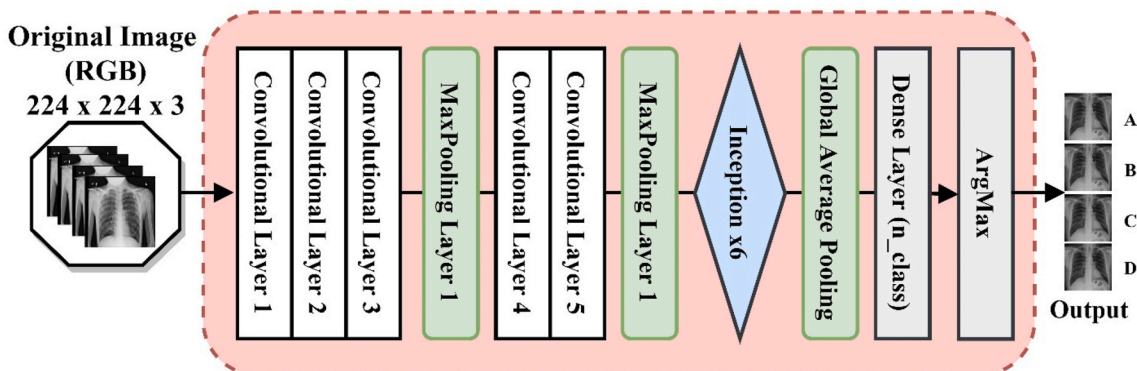
Fig. 2. The proposed model baseline Architecture is the Inception V3 variation proposed by Toda & Okuras [47].
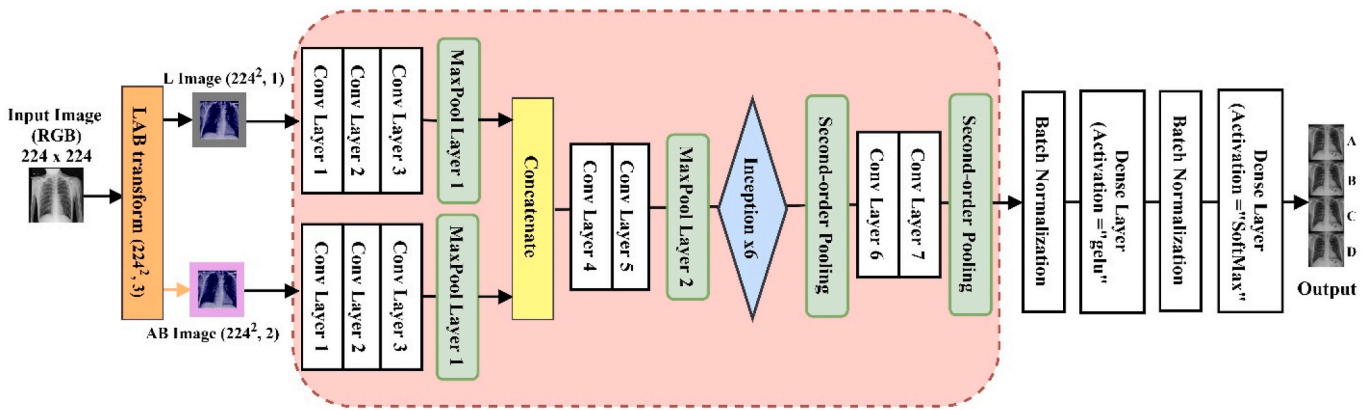
Fig. 3. The proposed model (LCSB-Inception). Seven 2D convolutional layers were used with size 3 x 3 except for the 4th convolutional layer with size 1 x 1. Second-order Pooling was used in place of conventional Max-pooling at the last two convolutional layers.
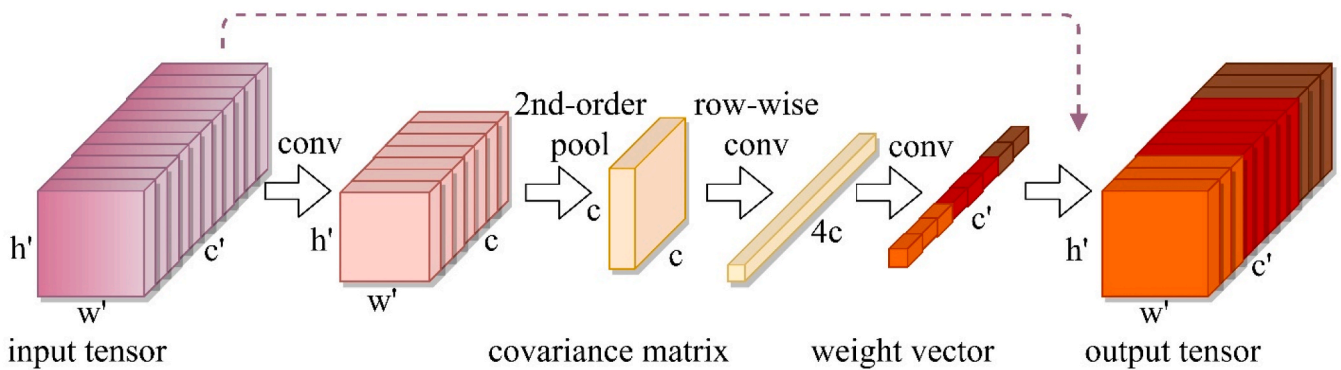
(a) Global second-order Pooling Block. After feature reduction, the second order block takes an input tensor and multiplies it along the channel dimension. It then computes the covariance matrix and performs two successive operations of a straight convolution and quasi activation.
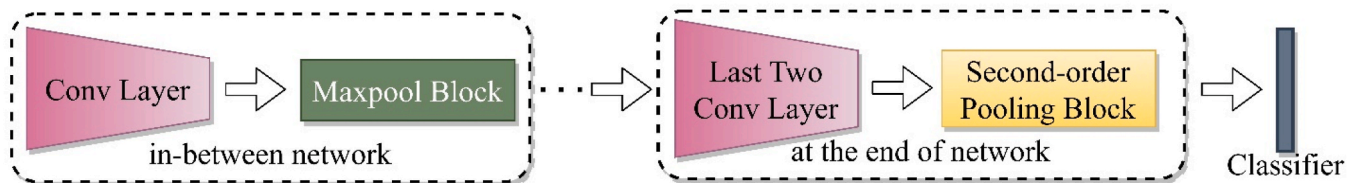
(b) Positioning of the Global second-order pooling in the proposed model

Fig. 4. The deployed second-order pooling. Our approach improves the network quasi-representation learning capabilities by modeling higher-order features of comprehensive images gotten from the dual channel convolutions.

two successive operations of convolution plus quasi activation for weight vector encoding, followed by a row-wise convolution for the likelihood function by treating each row as a group in group interpolation to preserve spatial features. Following that, a second convolution is performed, this time with a sigmoid function as a quadratic activation, producing a $c \times 1$ weight matrix. Finally, the appropriate element in the weight matrix is multiplied by each channel of the input tensor. Single channels are therefore softly accentuated or repressed in respect of weights.

Having mentioned earlier, this study tends to not only improve the feature extraction capabilities of deep learning network but also reduces the computational complexity of deep neural network which are not accepted in the medical sector for real-time implementation, Table 1 illustrates the reduction in the parameter of the proposed approach against the conventional inceptionV3. The first three convolutional

layers of the classic InceptionV3 architecture version comprise 32, 32, and 64 filters, respectively, for the filter distribution. According to the proportion of filters allocated to the L and AB branches, we have examined three variations of the two-branch architecture: 20%L–80% AB, 50%L–50%AB, and 80%L–20%AB. Table 2 displays the total number of filters for each variation, the weight savings and its Flop saving. The individual layers in each branch maintain the same number of filters as in the conventional InceptionV3 architecture since we were inspired by the original InceptionV3 architecture. The suggested model reduces weights and computational floating-point operations in the split layers by between 1/3 and 1/2. In this investigation, we used conditions that were 50% L + 50% AB.

Table 1

Illustrates the proposed model flow algorithm.

LCSB-Inception Model Algorithm
Step 1:
If input image is processed:
Print("Processed input image")
else:
Apply CLAHE Enhancement technique
Image.save
Step 2:
Initialize LCSB-Inception Model
If LCSB-Inception Model Input is CLAHE processed image:
Model accept input
else:
Print (error ...... "input image not preprocessed")
Initialize RGB image conversion
Apply LAB transform (L and AB channel)
while LCSB-Inception Model convolutional layer = Dual path
Path One accept L channel
Path Two accept AB Channel
end while
LCSB-Inception Model convolutional layer Dual path > 3
Concate Path one and Path two
Continue via single path with Convolution, pooling and activations layers
If last Convolution layers are the last two of the model:
Model apply Global second-order pooling layer
else:
Continue with maxpooling layers
While layer = classification layer
Model add()
Batch Normalization
Dense layer (Activate="gelu"),
Batch Normalization
Dense layer (Activate="SoftMax"),
End

Table 2

Filter Distributions and weights and required forward pass floating points operations along the first 3 convolutional layers of the baseline vs. the proposed model.

Model	1st & 2nd Layers	3rd Layer	Weights (Saving)	Flops (Saving)
baseline	32	64	28512	701 M
20%L + 80% AB	6–26	13–51	19746	485 M
50%L + 50% AB	16–16	32–32	14256	350 M
80%L + 20% AB	26–6	51–13	19566	481 M

4. Materials and experimental setup

This section covers the materials in terms of the dataset and the data enhancement techniques used in this study. Some existing works use proprietary datasets to evaluate their approaches, while others mix data from many publicly available sources. We used two publicly available datasets in this study. This section also covers the Evaluation metrics as well as the experimental setup of the proposed method.

4.1. Dataset and data enhancement

This study explains in detail the two deployed datasets in this section as well as the data enhancement techniques used. We choose these two publicly available datasets because they are more convenient to preprocess as well as have more than two classes. There are lots of binary classification datasets, however, few works have treated multi-classification as more challenging compared to binary classifications.

❖ **Dataset_1**: The ChestX-ray-15k dataset was acquired by Badawi et al. [51] from eleven different sources. This dataset contains a balanced amount of Chest X-ray images for training/validation and testing, with 3,500 and 1,500 images, respectively. The three unique chest X-ray categories are normal, COVID-19, and pneumonia. The images in this category are all in portable network graphics format, however at varied spatial resolutions. The validation set included 500 images from each test set class.

❖ **Dataset_2**: COVID-19 Radiography Dataset [52] comprises COVID-19, Lung Opacity, Normal and Pneumonia samples. It contains 3616 COVID-19 samples, 6012 Lung Opacity samples, 10,192 Normal samples and 1345 Pneumonia samples. Table 2 summarized the number of Samples used for training, validation and testing.

❖ **Data Enhancement**: In this study, the CLAHE [53] approach was considered a possible tool for doing image quality analyses. In contrast to conventional image processing techniques, the histogram

equalization approach generates the image histogram before cropping it and applying equalization. The noise contrast in the input image will likewise rise when the overall contrast of the image is increased during equalization. The input image is separated into small image fragments using the adaptive histogram equalization method, which is then enhanced by applying CLAHE to the regional fragments rather than the complete image. The mathematical formula for the histogram limit of each region is as follows:

$$\beta = \frac{M}{N}\left(1 - \frac{\alpha}{100}(S_{max} - 1)\right) \tag{1}$$

where *M* is the number of pixels in each area, *N* is its dynamic span, S_{max} is its highest permitted slope, and is a clip factor α that can vary from 0 to 100. This formula allows us to determine the clip limit β, which controls how much the image's contrast can shift.

The employed dataset is used to perform a multi-class prediction study for COVID-19 detection and to address the multi-class scarcity problem. All of the images were scaled to 224 by 224 pixels using bilinear interpolation. To increase the number of images in each class, the data transformations zoom range = 0.2, rotation range = 1, and horizontal flip = True were carried out. For each of the classes, Fig. 5 displays multiple illustrations of different visual views. The distribution splits of the dataset by class are shown in Table 3. For each class, a random selection from the dataset is used to determine the training set, validation set, and testing set.

4.2. Evaluation metrics

Several assessment metrics were used to gauge how robust the proposed model was. ROC curve, PR curve, F1-score, specificity, accuracy, and precision. True Positive, False Positive, True Negative and False Negative are all abbreviated as TP, FP, TN, and FN, respectively. The probability curve created by plotting at various threshold levels is referred to as the ROC (Receiver Operating Characteristic). The following are the metrics we used;

$$Accuracy = \frac{TP + TN}{(TP + TN) + (FP + FN)} * 100 \tag{2}$$

$$Precision = \frac{TP}{TP + FP} * 100 \tag{3}$$

$$Specificity = \frac{TN}{N} * 100 = \frac{TN}{TN + FP} * 100 \tag{4}$$

$$Sensitivity = \frac{TP}{P} * 100 = \frac{TP}{TP + FN} * 100 \tag{5}$$

$$F_1\ score = \left(\frac{SEN^{-1} + PRC^{-1}}{2}\right)^{-1} = \frac{2 * TP}{2 * TP + FP + FN} \tag{6}$$

4.3. Experimental setup

This experiment was carried out on Desktop Computer with 64.0 GB RAM and an NVIDIA GEFORCE RTX-3060 12 GB graphics processing unit with a CPU (AMD RYZEN 9 5900X). This paper utilizes the open-source library of Keras and TensorFlow for the implementation. Table 4 summarized the training hyperparameters used in this study. This study further explored the effects of the following hyperparameters on the proposed model.

Loss Function: Simply put, the loss function calculates how well the model can forecast using a given set of inputs. The difference between the model's estimate using a set of specified values and the measured ground truth is the computed result, which is the loss or failure. Categorical cross-entropy loss function and categorical smooth loss function were employed in this study's analysis.

Learning Rate: The learning rate is a parameter that determines how much the model should modify each time the model weights are changed in response to the projected mistake. In this paper, the learning rates of 1×10^{-4} and 1×10^{-3} are explored.
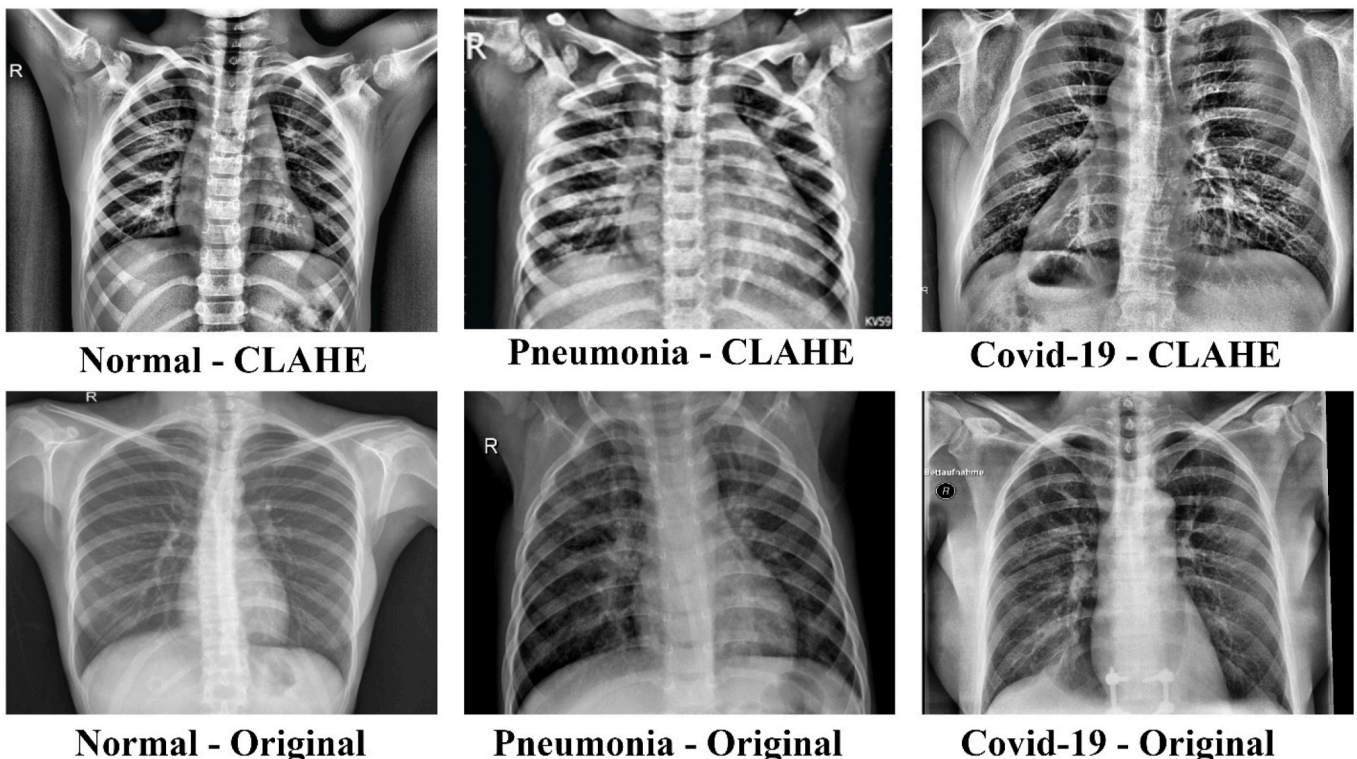
Fig. 5. Samples of the employed images. The upper column depicts the CLAHE processed image while the lower column depicts the corresponding original image.

Table 3
Employed dataset distribution.

	Partition	COVID-19	Lung Opacity	Normal	Pneumonia	T_{otal}	Total
Data_1	Training	3500	–	3500	3500	10500	15000
	Validation	500	–	500	500	1500	
	Testing	1000	–	1000	1000	3000	
Data_2	Training	3000	3000	3000	3000	12000	14400
	Validation	300	300	300	300	1200	
	Testing	300	300	300	300	1200	

Table 4
Experiment hyperparameters optimization and settings.

Hyperparameters and Settings				
Loss Function	Categorical Smooth Loss		Categorical Cross-Entropy	
Learning rate	0.0001	0.001	0.0001	0.001
Optimizer	Adam			
Batch size	8			
Reduce Learning Rate	0.2			
Epsilon	0.001			
Patience	10			
Verbose	1			
Es-Callback (Patience)	10			
Clip Value	0.2			
Epoch	100			
Input Size	(224 x 224)			

5. Results

The classification results cover the baseline experiment and the proposed model experiment. After the classification result follows the ablation studies and then we conclude the section with the state-of-the-art result comparison.

5.1. Classification results

This section discusses the classification results of the various approaches implemented in this paper. This section starts with the classification performance of the baseline model (Inception v3), followed by the proposed approach result with the employed datasets, down to the Ablation studies and lastly comparison with the state-of-the-art models.

5.1.1. Baseline experiment with Data_1(Inception v3)

This section discusses the baseline results on the original data vs the image enhancement technique (CLAHE) using the different experimental settings analyzed in this paper. The hyperparameters involved in this section include categorical smooth loss, categorical cross-entropy

loss function and 10^{-4} vs 10^{-3} learning rate. Table 5 records the classification performance results via accuracy, specificity, sensitivity, precision, F1-score and AUC. The learning rate of 10^{-3} with categorical cross-entropy loss recorded the least result with 0.92889 accuracy, 0.8934 sensitivity, 0.94656 specificity, 0.89955 precision, 0.89477 F1-score and 0.91983 AUC. Applying the CLAHE to the original image, the performance of the models improved with significant figures (+0.01 - +0.02). The best performance was seen at a learning rate of 10^{-4} and categorical smooth loss with an accuracy of 0.96533, the sensitivity of 0.94743, specificity of 0.97394, the precision of 0.94893, F1-score of 0.94789 and AUC of 0.96091 whereas the lowest performance was seen at the learning rate of 10^{-3} and categorical cross-entropy loss with an accuracy of 0.93956, the sensitivity of 0.90985, specificity of 095513, precision of 0.91099, F1-score of 0.90934 and 0.93269.

Table 6 shows the ROC and PR curves. We observe the model's performance in each class. The COVID-19 class had a better area in almost all the implemented parameters compared to the other class except for the performance recorded using the learning rate of 10^{-4} and categorical cross-entropy loss which the Pneumonia class (0.96) had the best area on the CLAHE image. The Normal and the Pneumonia class performance is based on the hyperparameters used. The best AP is seen at the learning rate of 10^{-4} and categorical_smooth_loss for the CLAHE image whereas the learning rate of 10^{-4} with the two learning rates yielding the same result. The AP results of the original input image have minimal improvement on the different hyperparameters with 0.01%. Figs. 6 and 7 summarizes the baseline result. The model recorded best performance on both Raw and CLAHE enhanced images were graphically illustrated for easy visualization.

5.1.2. Proposed model Data_1 classification result

We analyzed the model performance with the raw image vs the CLAHE processed and recorded their performance in Table 7. The best classification performance is seen at the learning rate of 10^{-3} and categorical_smooth_loss function for both raw input image and the CLAHE processed input image whereas their least performance result is seen at the learning rate of 10^{-4} and categorical cross-entropy loss function.

Table 5
Baseline classification Result. Learning rate; 10^{-4} and 10^{-3}, Loss function; Categorical_smooth_loss and categorical cross-entropy.

Image Type	Accuracy (%)	Sensitivity (%)	Specificity (%)	Precision (%)	F1 Score	AUC
Learning Rate: 10^{-4}, Loss Function: categorical_smooth_loss						
Raw Image	0.94044	0.91036	0.95515	0.91462	0.91138	0.93272
CLAHE Image	0.96533	0.94743	0.97394	0.94893	0.94789	0.96091
Learning Rate: 10^{-3}, Loss Function: categorical_smooth_loss						
Raw Image	0.93689	0.90393	0.95305	0.9078	0.90443	0.92957
CLAHE Image	0.95556	0.93335	0.96657	0.93574	0.93392	0.94986
Learning Rate: 10^{-4}, Loss Function: categorical cross-entropy						
Raw Image	0.94044	0.91033	0.95596	0.91301	0.91013	0.93394
CLAHE Image	0.944	0.91591	0.95834	0.91603	0.91565	0.93751
Learning Rate: 10^{-3}, Loss Function: categorical cross-entropy						
Raw Image	0.92889	0.8934	0.94656	0.89955	0.89477	0.91983
CLAHE Image	0.93956	0.90985	0.95513	0.91099	0.90934	0.93269

Table 6

Receiver Operating Characteristic (ROC) and Precision-Recall (PR) of the baseline model. Parameter employed includes Learning rate; 10^{-4} and 10^{-3}, Loss function; Categorical_smooth_loss and categorical cross-entropy.

ROC (Area)	Macro-Average	Micro-Average	COVID-19	Normal	Pneumonia
Learning Rate: 10^{-4}, Loss Function: categorical_smooth_loss					
Raw Image	0.93	0.93	0.95	0.92	0.93
CLAHE Image	0.96	0.96	0.97	0.95	0.96
Learning Rate: 10^{-3}, Loss Function: categorical_smooth_loss					
Raw Image	0.93	0.93	0.96	0.91	0.92
CLAHE Image	0.95	0.95	0.96	0.94	0.96
Learning Rate: 10^{-4}, Loss Function: categorical cross-entropy					
Raw Image	0.93	0.93	0.95	0.92	0.94
CLAHE Image	0.94	0.94	0.94	0.92	0.96
Learning Rate: 10^{-3}, Loss Function: categorical cross-entropy					
Raw Image	0.92	0.92	0.93	0.90	0.93
CLAHE Image	0.93	0.93	0.95	0.91	0.94

Precision-Recall (AP)	Micro-Average	COVID-19	Normal	Pneumonia
Learning Rate: 10^{-4}, Loss Function: categorical_smooth_loss				
Raw Image	0.86	0.90	0.80	0.88
CLAHE Image	0.92	0.93	0.88	0.94
Learning Rate: 10^{-3}, Loss Function: categorical_smooth_loss				
Raw Image	0.85	0.91	0.77	0.87
CLAHE Image	0.89	0.91	0.85	0.93
Learning Rate: 10^{-4}, Loss Function: categorical cross-entropy				
Raw Image	0.86	0.90	0.78	0.89
CLAHE Image	0.87	0.88	0.80	0.91
Learning Rate: 10^{-3}, Loss Function: categorical cross-entropy				
Raw Image	0.83	0.86	0.76	0.89
CLAHE Image	0.86	0.89	0.79	0.90

However, the CLAHE processed input image performed better than the raw input image with a percentage difference of +0.004 to +0.01. The optimal performance yielded an accuracy of 0.97867, the sensitivity of 0.96786, specificity of 0.984, precision of 0.96803, F1-Score of 0.90284, and AUC of 0.92924 for the CLAHE processed input image whereas the raw input image optimal performance yielded an accuracy of 0.97422, sensitivity of 0.961, specificity of 0.98047, precision of 0.9624, F1-Score of 0.96152 and AUC 0.9707.

Table 8 recorded the ROC and PR performance of the model. The ROC had a minimal increase in the area when the raw input image is enhanced using the CLAHE enhancement technology. The COVID-19 and the Pneumonia class had the best area (0.98) but in a different training setting. For both raw input image and CLAHE enhanced image, the optimal ROC area is seen at the learning rate of 10^{-3} and categorical_smooth_loss function while the worst is seen at the learning rate of 10^{-3} and categorical cross-entropy loss. The AP result is in line with the ROC result. However, the Pneumonia class had the best AP (0.96). followed by the COVID-19 class (0.95) and then the Normal class (0.93).

Fig. 8 shows the optimal performance settings ROC and PR curves of the implemented model whereas Fig. 9 shows the graphical performance result of the optimal settings of the model. We plotted the optimal classification performance of the model using the categorical_smooth_loss function in Fig. 9. Setting_A depicts the model's performance on the raw input image using Adam optimizer, learning rate 10^{-3} and while Setting_B depicts the CLAHE enhanced image. We further plotted the categorical cross-entropy function optimal classification performance alongside the categorical_smooth_loss function. Setting_C depicts the model's performance on the raw input image using the learning rate of 10^{-3} while Setting_D depicts the CLAHE enhanced image

5.1.3. Proposed model Data_2 classification result

The data_2 performance analysis is presented in this section. Just as in the case of Data_1, the categorical smooth loss and the categorical cross-entropy loss were experimented on using the learning rate of 10^{-4}
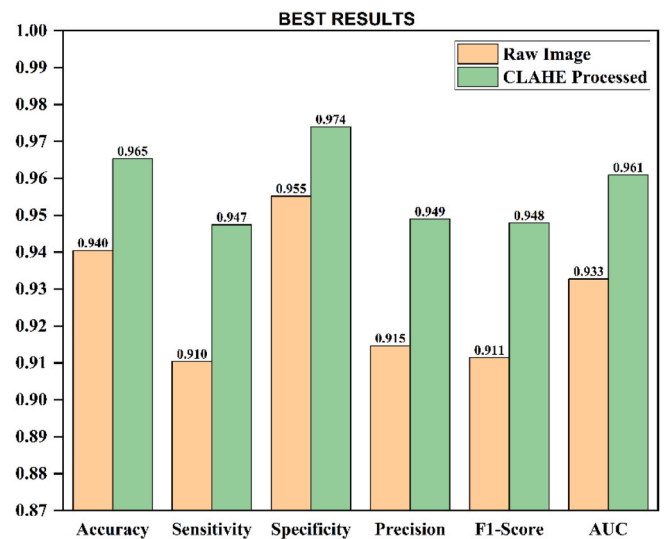
Fig. 7. Summary of the baseline classification performance of the plotted ROC and PR curves in Fig. 4.

A   B   C   D
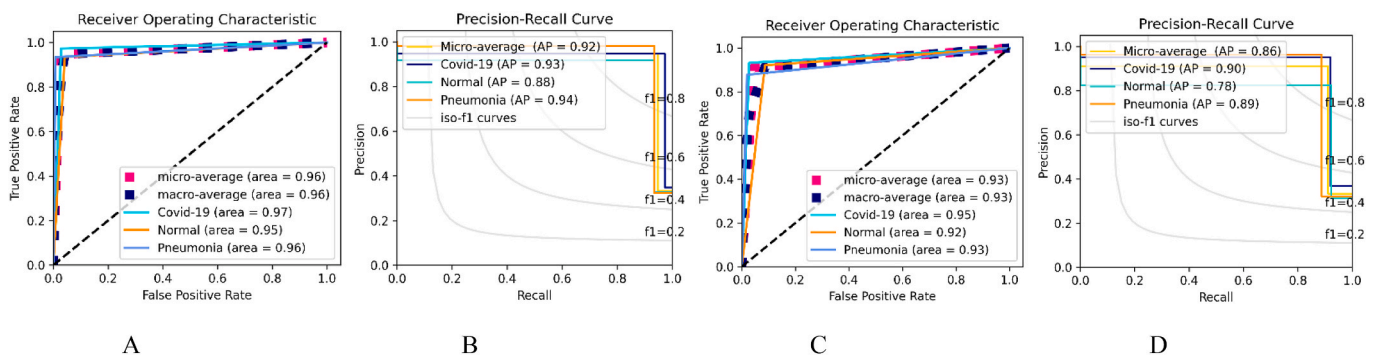
Fig. 6. The selected best ROC and Precision-Recall Curve of the implemented optimizers on the original data vs the CLAHE enhanced data. A & B depicts the CLAHE enhanced image ROC and AP while C & D depicts the Raw image ROC and AP via 10^{-4} Learning Rate and categorical_smooth_loss function.

Table 7

Proposed Model classification result on Data_1. Learning rate; 10^{-4} and 10^{-3}, Loss function; Categorical_smooth_loss and categorical cross-entropy.

Image Type	Accuracy (%)	Sensitivity (%)	Specificity (%)	Precision (%)	F1 Score	AUC
Learning Rate: 10^{-4}, Loss Function: categorical_smooth_loss						
Raw Image	0.95111	0.92693	0.96355	0.92656	0.92635	0.94532
CLAHE Image	0.95467	0.93114	0.96587	0.93658	0.93066	0.94881
Learning Rate: 10^{-3}, Loss Function: categorical_smooth_loss						
Raw Image	0.97422	0.961	0.98047	0.9624	0.96152	0.9707
CLAHE Image	0.97867	0.96786	0.984	0.96803	0.96787	0.976
Learning Rate: 10^{-4}, Loss Function: categorical cross-entropy						
Raw Image	0.92356	0.88615	0.94285	0.89449	0.88529	0.91428
CLAHE Image	0.93689	0.90514	0.95283	0.91141	0.90284	0.92924
Learning Rate: 10^{-3}, Loss Function: categorical cross-entropy						
Raw Image	0.95556	0.9333	0.96665	0.93436	0.9335	0.94998
CLAHE Image	0.968	0.95203	0.97594	0.95234	0.95208	0.96391

Table 8

Receiver Operating Characteristic (ROC) and Precision-Recall (PR) of the proposed model classification Result. Parameter employed includes Learning rate; 10^{-4} and 10^{-3}, Loss function; Categorical_smooth_loss and categorical cross-entropy.

ROC (Area)	Macro-Average	Micro-Average	COVID-19	Normal	Pneumonia
Learning Rate: 10^{-4}, Loss Function: categorical_smooth_loss					
Raw Image	0.95	0.95	0.94	0.93	0.96
CLAHE Image	0.95	0.95	0.96	0.91	0.98
Learning Rate: 10^{-3}, Loss Function: categorical_smooth_loss					
Raw Image	0.97	0.97	0.97	0.96	0.98
CLAHE Image	0.98	0.98	0.98	0.97	0.98
Learning Rate: 10^{-4}, Loss Function: categorical cross-entropy					
Raw Image	0.91	0.91	0.89	0.90	0.96
CLAHE Image	0.93	0.93	0.95	0.88	0.97
Learning Rate: 10^{-3}, Loss Function: categorical cross-entropy					
Raw Image	0.95	0.95	0.95	0.95	0.95
CLAHE Image	0.96	0.96	0.97	0.96	0.96

Precision-Recall (AP)	Micro-Average	COVID-19	Normal	Pneumonia
Learning Rate: 10^{-4}, Loss Function: categorical_smooth_loss				
Raw Image	0.88	0.86	0.87	0.92
CLAHE Image	0.89	0.87	0.86	0.94
Learning Rate: 10^{-3}, Loss Function: categorical_smooth_loss				
Raw Image	0.94	0.94	0.91	0.96
CLAHE Image	0.95	0.95	0.94	0.95
Learning Rate: 10^{-4}, Loss Function: categorical cross-entropy				
Raw Image	0.82	0.84	0.75	0.89
CLAHE Image	0.85	0.83	0.81	0.91
Learning Rate: 10^{-3}, Loss Function: categorical cross-entropy				
Raw Image	0.89	0.92	0.87	0.90
CLAHE Image	0.92	0.95	0.94	0.95

and 10^{-3} as shown in Table 9. The learning rate of 10^{-4} to be the optimal setting for the two losses used. However, the categorical_smooth_loss performance had the overall classification performance with an accuracy of 0.97236, the sensitivity of 0.94474, specificity of 0.98156, precision of 0.94602, F1-Score of 0.94513 and AUC of 0.9315 on the raw

image whereas when enhanced with the CLAHE image enhancement technique, the proposed model best performance results were 0.98199 accuracy, 0.96407 sensitivity, 0.98798 specificity, 0.9651 precision, 0.96414 F1-Score and 0.97603 AUC. To validate the classification performance result, the Precision-recall curve and Receiver Operating Characteristics were used to measure the individual class performance of the model. The PR curve shows the Average precision whereas the ROC shows the area. The COVID-19 class and the Pneumonia class had a general better Area compared to the Lung opacity and Normal class with an area of 0.99 on the learning rate of 10^{-4} and categorical_smooth_loss. The best AP is as well recorded at the learning rate of 10^{-4} and categorical_smooth_loss training setup. Different from the Area, the Pneumonia class had a better AP, followed by the COVID-19 class, the Lung opacity and the normal class with an AP of 0.99, 0.97, 0.90, and 0.90 respectively.

Fig. 10 shows the graphical illustration of the DAT_2 classification performance using the ROC and Precision-Recall curve. This study chose to show only the optimal training setting performance for both the raw input image and CLAHE enhanced image. As noted in Table 8, the optimal training setting is seen at the learning rate of 10^{-4} and categorical_smooth_loss for both input scenarios. This study explored the classification performance of the proposed model on data_2 graphically in Fig. 11. All the experimented setting results were recorded on the graph to guide readers on the contribution of each setting to our model performance.

5.2. Ablation studies of the implemented models

The Ablation studies of our proposed model are analyzed quantitively using the accuracy, sensitivity, specificity, precision, F1-score and AUC score performance metrics as shown in Table 10. The evaluation is based on four approaches, the baseline performance which is the conventional InceptionV3, the baseline architecture with CLAHE enhanced image, the proposed method with the raw input image and the proposed method on the CLAHE enhanced image. The reason for this quantitative ablation study is to estimate the usefulness of our proposed approach. The optimal performance of the proposed approach on the two experimented datasets was used for the quantitative study. For the Data_1, the optimal performance is seen in the training settings of 10^{-3} and categorical smooth loss function whereas that of Data_2 is seen at the training settings of 10^{-4} and categorical smooth loss function. For the Data_1, the proposed approach with raw input image improved the baseline performance with +0.03733 accuracy, +0.05707 sensitivity, +0.02742 specificity, +0.0546 precision, +0.05709 F1-score and +0.04113 AUC score. however, enhancing the image with the CLAHE image enhancement technique further improved the proposed model classification performance with +0.04178 accuracy, +0.06393
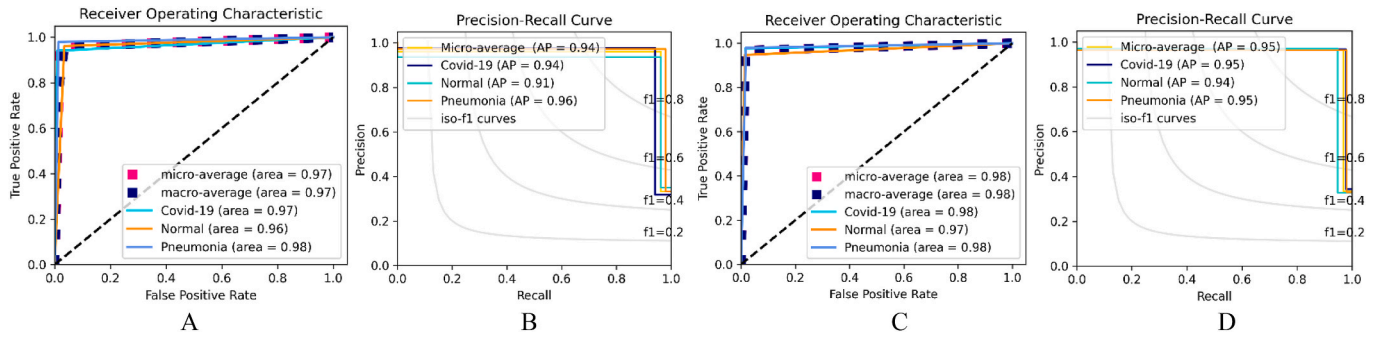
Fig. 8. The selected best ROC and Precision-Recall Curve of the implemented optimizers on the raw input image vs the CLAHE enhanced image. A & B depicts the ROC and AP of the Raw image while C & D depicts the ROC and AP of the CLAHE enhanced Image.
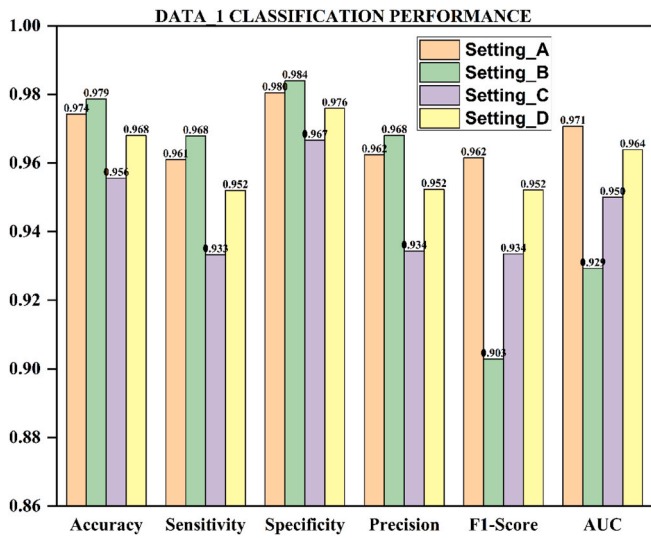
Fig. 9. Graphical illustration of the proposed model classification performance. Setting_A, B, C and D depict the classification performance results on both raw input image and CLAHE enhanced image.

sensitivity, +0.03095 specificity, +0.06023 precision, +0.06344 F1-Score, and +0.04643 AUC score. Multiclass classification is a difficult task compared to binary classification. The more the number of classes the more difficult it is for models to perform well. Comparing the baseline result of Data_1 against Data_2, we saw that the baseline result decreased from − 0.1178 to − 0.04367 of the employed evaluation metrics. For the Data_2, the proposed approach with raw input image improved the baseline performance with +0.03579 accuracy, +0.15863 sensitivity, +0.05282 specificity, +0.13617 precision, +0.15544 F1-score and +0.10572 AUC score. however, enhancing the image with the CLAHE image enhancement technique further improved the proposed model classification performance with +0.08877 accuracy, +0.17795 sensitivity, +0.05924 specificity, +0.15525 precision, +0.17445 F1-Score, and +0.1186 AUC score.

6. Result discussion

Table 11 shows the performance of various state-of-the-art deep learning models which are all single-path approaches. We first removed their classification heads and finetuned them to correspond to the number of classes in Data_2. The analyzed models include, DenseNet101, EfficientNetB7, GoogleNet, InceptResNetV2, VGG16, Xception, ResNet50, InceptionV3 and our proposed two path models. First, the computational cost of the models is on the high side thus making it impossible for real-time implementation. Our proposed approach was to tackle not only the recognition accuracy but also to reduce the

computational cost and extract accurate features of the input image form classifications. Convolutional neural networks (CNNs) have seen considerable growth over the last decade in solving several challenges in computer vision. CNN's are incredibly cost expensive because they explore the image-to-image invariance, which is essential for training deep learning models and avoiding extreme overfitting. Despite its enormous achievement, its computational complexity continues to limit the use of embedded devices, especially in the medical field.

Downsampling input images to fewer qualities is a common technique for lowering the computation complexity. In this study, we trained the pre-trained models with the same training setting as our proposed model. Here we used data_2 since it has more classes than Data_3. Multiclassification is a difficult task compared to binary or fewer class settings. We employed the same evaluation metrics for a fair comparison. Among the pre-trained models, the DenseNet201 with an accuracy of 0.96. The deployed pretrained all yielded nice results however the EfficientNetB7 and the ResNet50 yield below 90% accuracy.

We make a significant contribution from a fresh angle by proposing an alternative to the default convolution module, which can result in models with even better generalization abilities and/or parameter efficiency. The proposed idea of Dual path and replacement of max pooling with global second-order pooling are intended to augment visual features by extracting information from multiple inputs at various resolutions. The proposed model performed much better than the conventional models with an accuracy of 0.98199, sensitivity of 0.96407, specificity of 0.98798, precision of 0.96510, F1-score of 0.96414 and AUC of 0.97603. In terms of weight saving and flop saving, the proposed approach served up to 14256 wt and flop of 350 M of the conventional InceptionV3.

6.1. Comparison with the state-of-the-art deep learning models

This section compares the performance result of the proposed models with the state-of-the-art results (2021–2022) as shown in Table 12. The comparison is based on multiclass models (3 classes and 4 classes) for a fair comparison. Hussain et al. [54], performed a dual multiclass experiment (3 classes and 4 classes) with a novel CNN approach termed CoroDet and achieved an accuracy of 94.2 for the three classes and 91.2 for the four classes. Da et al. [11], employed several approaches for Covid-19 detection such as from scratch CNN, finetuned VGG-16 and ResNet50. Among the implemented models, the VGG-16 model recorded the highest accuracy, followed by the ResNet50 and CNN with an accuracy of 97.7, 96.4 and 93.7 respectively. Jadon et al. [55], used another approach called the Siamese Network and compared his result with a CNN approach (VGG-16 via transfer learning). Although the proposed Siamese approach via Transfer learning recorded the best results in terms of accuracy, precision, recall and F1-score, the issues of Computational complexity of the model supersedes the CNN approach. Jadon et al. [55], recorded an accuracy of 96.4, precision of 96.5, a recall of 96.2 and an F1-score of 95.9.

Table 9

Proposed Model classification Result.

Image Type	Accuracy (%)	Sensitivity (%)	Specificity (%)	Precision (%)	F1 Score	AUC
Learning Rate: 10^{-4}, Loss Function: categorical_smooth_loss						
Raw Image	0.97236	0.94475	0.98156	0.94602	0.94513	0.96315
CLAHE Image	0.98199	0.96407	0.98798	0.9651	0.96414	0.97603
Learning Rate: 10^{-3}, Loss Function: categorical_smooth_loss						
Raw Image	0.96985	0.93965	0.97988	0.94193	0.94012	0.95977
CLAHE Image	0.97069	0.94138	0.98043	0.94379	0.94174	0.96091
Learning Rate: 10^{-4}, Loss Function: categorical cross-entropy						
Raw Image	0.96231	0.92465	0.97485	0.9262	0.925	0.94975
CLAHE Image	0.97697	0.95393	0.98462	0.95554	0.95425	0.96928
Learning Rate: 10^{-3}, Loss Function: categorical cross-entropy						
Raw Image	0.96943	0.93876	0.9796	0.94262	0.9395	0.95918
CLAHE Image	0.97529	0.95056	0.98351	0.95237	0.95097	0.96704
ROC (Area)	**Macro-Average**	**Micro-Average**	**COVID-19**	**Lung Opacity**	**Normal**	**Pneumonia**
Learning Rate: 10^{-4}, Loss Function: categorical_smooth_loss						
Raw Image	0.96	0.96	0.97	0.97	0.94	0.97
CLAHE Image	0.98	0.98	0.99	0.97	0.95	0.99
Learning Rate: 10^{-3}, Loss Function: categorical_smooth_loss						
Raw Image	0.95	0.95	0.95	0.96	0.92	0.97
CLAHE Image	0.96	0.96	0.98	0.97	0.93	0.96
Learning Rate: 10^{-4}, Loss Function: categorical cross-entropy						
Raw Image	0.96	0.96	0.96	0.97	0.94	0.96
CLAHE Image	0.97	0.97	0.98	0.98	0.95	0.97
Learning Rate: 10^{-3}, Loss Function: categorical cross-entropy						
Raw Image	0.96	0.96	0.96	0.97	0.95	0.95
CLAHE Image	0.97	0.97	0.98	0.97	0.95	0.96
Precision-Recall (AP)	**Micro-Average**	COVID-19	Lung Opacity	Normal	Pneumonia	
Learning Rate: 10^{-4}, Loss Function: categorical_smooth_loss						
Raw Image	0.91	0.90	0.93	0.84	0.96	
CLAHE Image	0.94	0.97	0.90	0.90	0.99	
Learning Rate: 10^{-3}, Loss Function: categorical_smooth_loss						
Raw Image	0.87	0.87	0.88	0.80	0.95	
CLAHE Image	0.90	0.95	0.89	0.83	0.94	
Learning Rate: 10^{-4}, Loss Function: categorical cross-entropy						
Raw Image	0.90	0.92	0.91	0.84	0.94	
CLAHE Image	0.92	0.96	0.91	0.87	0.96	
Learning Rate: 10^{-3}, Loss Function: categorical cross-entropy						
Raw Image	0.90	0.91	0.93	0.83	0.93	
CLAHE Image	0.92	0.94	0.92	0.86	0.95	
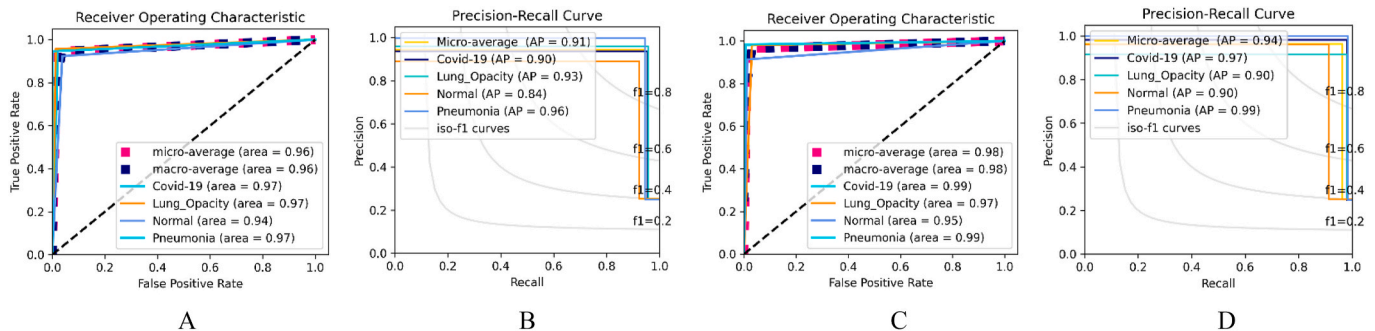
Fig. 10. Graphically representation (ROC and Precision-Recall Curve of the raw input image vs the CLAHE enhanced image) of the best training setting on Data_2. A & B depicts the ROC and AP of the Raw image while C & D depicts the ROC and AP of the CLAHE enhanced Image.
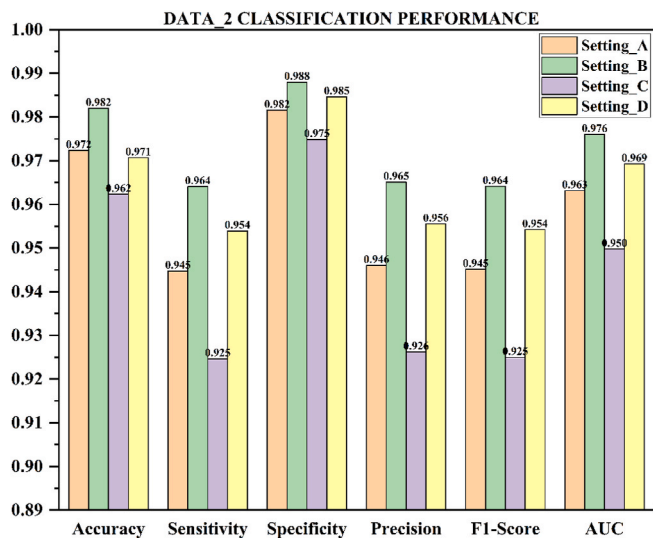
Fig. 11. Graphical illustration of the proposed model's best classification performance on the two-loss functions using Data_2. Setting_A and B depict the performance of the model using the Learning rate of 10^{-4} and categorical_smooth_loss while Setting_C and C depict the learning rate of 10^{-4} and categorical cross-entropy loss function performance on both raw input image and CLAHE enhanced image.

Aggarwal et al. [56], fine-tuned eight deep learning models for the task of Covid-19 detection using a dual dataset (3 classes and 4 classes). Th result shows that the higher the number of classes in a dataset, the more difficult it is for models to perform better as models with three classes dataset experiment recorded better results than four classes dataset. However, the DenseNet201 recorded the best result with an accuracy of 97.0 while the InceptionV3 recorded the lowest result with an accuracy of 90.0 on the three-class dataset experiment. For the four classes experiment, the MobileNetv2, Xception, and ResNet50v2 recorded the best result with an accuracy of 81.0 while the InceptionV3 still

recorded the lowest with an accuracy of 70.0. Luz et al. [44] and Perumal et al. [57] also employed the Transfer learning approach for COVID-19 detection, however, their approach recorded poor accuracy. Employing the use of an attention mechanism-based transformer which is the recent breakthrough in computer vision tasks, Shome et al. [58], proposed the use of a COVID-Transformer for the detection of COVID-19. However, the proposed approach had a 92.0 in accuracy, 93.0 in precision, 89.0 in recall and 91.0 in F1-score. The yielded result is caused by the number of training sets as transformer models require huge training samples for optimal performance. In regards to the computational cost, transformers are heavy models and thus need more focus on their computational complexity if they are to be used in the medical sector.

Huang et al. [59], just as Aggarwal et al. [56], employed seven pre-trained deep learning models in two scenarios. First finetuning without focusing on the reduction of the computational complexity of the models and secondly, he focused on the computational complexity of the models. From his recorded results, we saw that the reduced model computational complexity recorded better results compared to the conventional model which is a headway in the medical sector. In line with his idea of building models with a less computational cost yet yielding higher accuracy and precision, we developed our LCSB model which superseded all the compared models in terms of accuracy and computational complexity of the models. The proposed model recorded an accuracy of 97.9, precision of 96.8, a recall of 97.6 and an F1-score of 96.8 for the three-class dataset and an accuracy of 98.2, precision of 96.5, recall of 97.6, and f1-score of 96.4 for the four-class dataset. In conclusion, our proposed models showed the greatest degree of precision, indicating that the proposed classifier seldom misclassifies negative samples as positive values. The classifier can recognize the majority of positive samples that belong to each class, as evidenced by the fact that we obtained the highest recall score. When compared to baseline techniques, the recommended method has the highest F1 score, which suggests that it is the most balanced in terms of precision and sensitivity.

Table 10
Quantitative Ablation studies of the proposed model performance.

Type	Accuracy (%)	Sensitivity (%)	Specificity (%)	Precision (%)	F1 Score	AUC
Data_1: Learning Rate: 10^{-3}, Loss Function: categorical_smooth_loss						
Baseline + Raw Image	0.93689	0.90393	0.95305	0.9078	0.90443	0.92957
Baseline + CLAHE	+0.01867	+0.02942	+0.01352	+0.02794	+0.02949	+0.02029
Proposed + Raw Image	+0.03733	+0.05707	+0.02742	+0.0546	+0.05709	+0.04113
Proposed + CLAHE	+0.04178	+0.06393	+0.03095	+0.06023	+0.06344	+0.04643
Data_2: Learning Rate: 10^{-4}, Loss Function: categorical_smooth_loss						
Baseline + Raw Image	0.89322	0.78612	0.92874	0.80985	0.78969	0.85743
Baseline + CLAHE	+0.01423	+0.02862	+0.00951	+0.0182	+0.02761	+0.01907
Proposed + Raw Image	+0.03579	+0.15863	+0.05282	+0.13617	+0.15544	+0.10572
Proposed + CLAHE	+0.08877	+0.17795	+0.05924	+0.15525	+0.17445	+0.1186

Table 11
Pretrained model performance.

Models	Accuracy (%)	Sensitivity (%)	Specificity (%)	Precision (%)	F1 Score	AUC
Data_2, Loss: Categorical_smooth_loss, Learning Rate: 10^{-4}						
DenseNet201	0.96000	0.91981	0.97325	0.92453	0.92088	0.94651
EfficientNetB7	0.87333	0.74787	0.91542	0.83094	0.73639	0.83164
GoogleNet	0.93000	0.86024	0.95322	0.86795	0.86188	0.90673
InceptResNetV2	0.94667	0.89385	0.96434	0.90298	0.89398	0.92910
VGG16	0.91000	0.81988	0.93985	0.87301	0.82008	0.87986
Xception	0.90000	0.80032	0.93315	0.83420	0.80144	0.86674
ResNet50	0.89322	0.78612	0.92874	0.80985	0.78969	0.85743
InceptionV3	0.90745	0.81474	0.93825	0.82805	0.81730	0.87650
Proposed Model	0.98199	0.96407	0.98798	0.96510	0.96414	0.97603

Table 12
State-of-the-art model result comparison.

Ref/Year	Nos. Classes	Model	Accuracy	Precision	Recall	F1-Score
E. Hussain et al., 2021 [54]	3 Classes	Novel CNN Model CoroDet	94.2	–	–	–
	4 Classes		91.2	–	–	–
S. K Das et al., 2021 [11]	3 Classes	CNN	93.7	–	–	–
		VGG-16	97.7	–	–	–
		ResNet50	96.4	–	–	–
S. Jadon et al., 2021 [55]	3 Classes	Logistic Regression	82.4	82.2	82.8	82.8
		Convolutional Neural Network	90.2	91.2	90.1	90.4
		Transfer Learning (VGG16)	93.3	93.1	93.2	92.8
		Siamese Networks	94.6	94.5	94.1	94.7
		Siamese Networks (Transfer Learning)	96.4	96.5	96.2	95.9
S. Aggarwal et al., 2021 [56]	3 Classes	DenseNet121	97.0	–	–	–
		Xception	96.0	–	–	–
		MobileNetv2	95.0	–	–	–
		ResNet50v2	94.0	–	–	–
		NASNetMobile	93.0	–	–	–
		VGG19	92.0	–	–	–
		InceptionResNetv2	92.0	–	–	–
		Inceptionv3	90.0	–	–	–
	4 Classes	MobileNetv2	81.0	–	–	–
		Xception	81.0	–	–	–
		ResNet50v2	81.0	–	–	–
		DenseNet121	77.0	–	–	–
		InceptionResNetv2	76.0	–	–	–
		VGG19	75.0	–	–	–
		NASNetMobile	75.0	–	–	–
		Inceptionv3	70.0	–	–	–
E. Luz et al., 2021 [44]	3 Classes	EfficientNet-B0	89.0	88.0	89.0	88.0
V. Perumal et al., 2021 [57]	3 Classes	VGG-16	87.0	87.0	85	86.0
D. Shome et al., 2021 [58]	3 Classes	COVID-Transformer	92.0	93.0	89.0	91.0
M.-L. Huang et al., 2022 [59]	3 Classes (First Approach)	InceptionV3	96.5	96.7	96.8	96.7
		ResNet50v2	95.1	95.2	95.1	95.1
		Xception	95.9	96.5	96.0	96.5
		DenseNet121	94.7	94.7	94.6	95.0
		MobileNetV2	96.4	96.3	96.3	96.0
		EfficientNet-B0	94.8	94.5	94.5	94.5
		EfficientNetV2-S	94.8	94.8	94.8	94.6
	3 Classes (Second Approach)	InceptionV3	97.7	96.7	96.7	96.8
		ResNet50v2	97.1	96.8	96.9	96.9
		Xception	97.3	96.5	96.4	96.2
		DenseNet121	95.4	95.1	95.3	95.2
		MobileNetV2	97.7	96.6	96.7	96.4
		EfficientNet-B0	96.8	96.7	96.6	96.6
		EfficientNetV2-S	96.7	96.8	96.8	96.7
Ours 2022	3 classes	**Proposed LCSB-Inception**	**97.9**	**96.8**	**97.6**	**96.8**
	4 classes		**98.2**	**96.5**	**97.6**	**96.4**
		DenseNet201	96.0	92.0	91.9	92.0
		InceptResNetV2	94.6	90.2	89.4	89.4
		GoogleNet	93.0	86.8	86.0	86.2
		VGG16	91.0	87.3	81.9	82.0
		InceptionV3	90.7	82.8	81.5	81.7
		Xception	90.0	83.4	80.0	80.1
		ResNet50	89.3	81.0	78.6	79.0
		EfficientNetB7	87.3	83.1	75.1	74.0

6.2. Limitations and future works

This paper identified some limitations of the proposed approach. The severity of COVID-19 illness was not considered a sub-classification (mild, moderate, or severe disease). We also observe that the chest X-ray dataset only shows one series for a patient, supporting the claim made by Ref. [33] that a small dataset (one chest x-ray series for a patient) cannot be used to predict whether a patient would develop a radiographic abnormality as the disease advances. Furthermore, this paper implemented only the CLAHE image enhancement techniques whereas there are lots of image enhancement techniques proposed by various researchers which have yielded better performance. As a future study, this study will address the highlighted shortcomings. More Image enhancement techniques such as Multi-Scale Retinex with Color Restoration (MSRCR), Multi-Scale Retinex with chromaticity preservation (MSRCP), etc. as well as other medical image modalities will be used to assess the robustness of the model in medical image disease classification. Lastly, we will extend the proposed approach using other deep learning pre-trained models as a baseline.

7. Conclusion

In this study, a new LCSB-Inception; a two-path (L and AB channel) Inception V3 network along the first three convolutional layers with a global second-order pooling at the last two convolutional layers is proposed for early detection and accurate feature extraction of Chest X-ray images with less computational complexity for COVID-19 detection. The proposed model is experimented on a publicly available dataset ChestX-ray-15k dataset (Data_1) and COVID-19 Radiography dataset (Data_2) and evaluated using accuracy, sensitivity, specificity, precision, F1-score and AUC evaluation metrics. The proposed model performance supports the claims of its robust feature extraction of the chest X-ray Images. The L channel (one branch) focused on the textural and edge features while the AB channel (second branch) focuses on the color properties of Chest

X-ray image features without sacrificing performance. The L achromatic channel and the AB channels filters are set to 50%L-50%AB thus saving between one-third and one-half of the parameters in the divided branches. In other to learn higher-order features for improving non-linear modeling capability, we replaced the max-pooling layer of the last two Convolutional layers with a global second-order pooling layer. The detection accuracy of the LCSB-Inception is further improved by employing the Contrast Limited Adaptive Histogram Equalization (CLAHE) image enhancement technique on the input image before feeding them to the network. According to the experimental results, the proposed models yielded an accuracy of 97.9 on Data_1 and an accuracy of 98.2 on Data_2 According to the results, the proposed models outperform traditional deep learning models and other state-of-the-art approaches described in the literature in terms of COVID-19 identification. A quantitative Ablation study is carried out to show the contribution of each step in the proposed model.

Code Availability/Availability of Data

Both https://github.com/abeerbadawi/COVID-ChestXray15k-Dataset-Transfer-Learning (retrieved: May 17, 2022) and and https://www.kaggle.com/datasets/tawsifurrahman/covid19-radiography-database (retrieved: 30 July 2022). provides access to the dataset utilized in this study. The TensorFlow/Keras code we utilized in our experiment is not currently accessible to the general public, but it will be when the study is published.

Ethical approval

This article does not contain any studies with human participants or animals performed by any of the authors.

Informed consent

Informed consent was obtained from all participants included in the study.

Declaration of competing interest

The authors declare that they have no known competing financial interests or personal relationships that could have appeared to influence the work reported in this paper.

Acknowledgments

References

[1] W. Yang, et al., Clinical characteristics and imaging manifestations of the 2019 novel coronavirus disease (COVID-19): a multi-center study in Wenzhou city, Zhejiang, China, J. Infect. 80 (4) (2020) 388–393, https://doi.org/10.1016/j.jinf.2020.02.016.

[2] M.K. Hasan, et al., Challenges of deep learning methods for COVID-19 detection using public datasets, Inform. Med. Unlocked 30 (2022), 100945, https://doi.org/10.1016/j.imu.2022.100945. February.

[3] S. Zaim, J.H. Chong, V. Sankaranarayanan, A. Harky, COVID-19 and multiorgan response, Curr. Probl. Cardiol. 45 (8) (2020), https://doi.org/10.1016/j.cpcardiol.2020.100618.

[4] C. Hani, et al., COVID-19 pneumonia: a review of typical CT findings and differential diagnosis, Diagnos. Intervent. Imag. 101 (5) (2020) 263–268, https://doi.org/10.1016/j.diii.2020.03.014.

[5] J. Zheng, SARS-coV-2: an emerging coronavirus that causes a global threat, Int. J. Biol. Sci. 16 (10) (2020) 1678–1685, https://doi.org/10.7150/ijbs.45053.

[6] J.A. Lewnard, N.C. Lo, Scientific and ethical basis for social-distancing interventions against COVID-19, Lancet Infect. Dis. 20 (6) (2020) 631–633, https://doi.org/10.1016/S1473-3099(20)30190-0.

[7] Y. Wang, H. Kang, X. Liu, Z. Tong, Combination of RT-qPCR testing and clinical features for diagnosis of COVID-19 facilitates management of SARS-CoV-2 outbreak, J. Med. Virol. 92 (6) (2020) 538–539, https://doi.org/10.1002/jmv.25721.

[8] Y. Li, et al., Stability issues of RT-PCR testing of SARS-CoV-2 for hospitalized patients clinically diagnosed with COVID-19, J. Med. Virol. 92 (7) (2020) 903–908, https://doi.org/10.1002/jmv.25786.

[9] T. Ai, et al., Correlation of chest CT and RT-PCR testing for coronavirus disease 2019 (COVID-19) in China: a report of 1014 cases, Radiology 296 (2) (2020), https://doi.org/10.1148/radiol.2020200642. E32–E40.

[10] R.C. Nelson, S. Feuerlein, D.T. Boll, New iterative reconstruction techniques for cardiovascular computed tomography: how do they work, and what are the advantages and disadvantages, J. Cardiovasc. Comput. Tomograph. 5 (5) (2011) 286–292, https://doi.org/10.1016/j.jcct.2011.07.001.

[11] S.K. Das, S. Bebortta, A study on geospatially assessing the impact of COVID-19 in Maharashtra, India, Egypt. J. Rem. Sens. Space Sci. 25 (1) (2022) 221–232.

[12] C.C. Ukwuoma, Q. Zhiguang, M.A. Hossin, B.M. Cobbinah, A. Oluwasanmi, I. A. Chikwendu, C.J. Ejiyi, H.S. Abubakar, Holistic attention on pooling based cascaded partial decoder for real-time salient object detection, in: 2021 4th International Conference on Pattern Recognition and Artificial Intelligence (PRAI), Aug. 2021, https://doi.org/10.1109/prai53619.2021.9551094.

[13] C.C. Ukwuoma, M.A. Hossain, J.K. Jackson, G.U. Nneji, H.N. Monday, Z. Qin, Multi classification of breast cancer lesions in histopathological images using DEEP_Pachi: multiple self-attention head, Diagnostics 12 (5) (May 2022) 1152, https://doi.org/10.3390/diagnostics12051152.

[14] C.C. Ukwuoma, Z. Qin, S.B. Yussif, M.N. Happy, G.U. Nneji, G.C. Urama, C. D. Ukwuoma, N.B. Darkwa, H. Agobah, Animal species detection and classification framework based on modified multiscale attention mechanism and feature pyramid network, Scientific African 16 (Jul. 2022), https://doi.org/10.1016/j.sciaf.2022.e01151 e01151.

[15] C.C. Ukwuoma, Q. Zhiguang, M.B. Bin Heyat, L. Ali, Z. Almaspoor, H.N. Monday, Recent advancements in fruit detection and classification using deep learning techniques, Math. Probl Eng. 2022 (Jan. 2022) 1–29, https://doi.org/10.1155/2022/9210947.

[16] P.K. Sethy, S.K. Behera, P.K. Ratha, P. Biswas, Detection of coronavirus disease (COVID-19) based on deep features and support vector machine, Int. J. Math. Eng. Manag. Sci. 5 (4) (2020) 643–651, https://doi.org/10.33889/IJMEMS.2020.5.4.052.

[17] A. Borkowski, Using artificial intelligence for COVID-19 chest X-ray diagnosis,, Fed. Pract. 37 (9) (2020), https://doi.org/10.12788/fp.0045.

[18] V. Chouhan, et al., A novel transfer learning-based approach for pneumonia detection in chest X-ray images, Appl. Sci. 10 (2) (2020), https://doi.org/10.3390/app10020559.

[19] P.R.A.S. Bassi, R. Attux, A deep convolutional neural network for COVID-19 detection using chest X-rays, Res. Biomed. Eng. 38 (1) (2022) 139–148, https://doi.org/10.1007/s42600-021-00132-9.

[20] W. Mingming, Multi-path Convolutional Neural Networks for Complex Image Classification, CoRR, 2015 abs/1506.04701. Available from: http://arxiv.org/abs/1506.04701.

[21] C. Yunpeng, L. Jianan, X. Huaxin, J. Xiaojie, Y. Shuicheng, F. Jiashi, Dual Path Networks, CoRR, 2017 abs/1707.01629. Available from: http://arxiv.org/abs/1707.01629.

[22] C. Szegedy, V. Vanhoucke, S. Ioffe, J. Shlens, Z. Wojna, Rethinking the inception architecture for computer vision, in: Proceedings of the IEEE Computer Society Conference on Computer Vision and Pattern Recognition, vol. 2016, Decem, 2016, pp. 2818–2826, https://doi.org/10.1109/CVPR.2016.308.

[23] R. M. Pereira, D. Bertolini, L. O. Teixeira, C. N. Silla, and Y. M. G. Costa, "COVID-19 identification in chest X-ray images on flat and hierarchical classification scenarios," Comput. Methods Progr. Biomed., vol. 194, 2020, doi: 10.1016/j.cmpb.2020.105532.

[24] P.K. Sethy, S.K. Behera, P.K. Ratha, P. Biswas, Detection of coronavirus disease (COVID-19) based on deep features and support vector machine, Int. J. Math. Eng. Manag. Sci. 5 (4) (2020) 643–651, https://doi.org/10.33889/IJMEMS.2020.5.4.052.

[25] H. Nasiri, S. Hasani, Automated detection of COVID-19 cases from chest X-ray images using deep neural network and XGBoost, Radiography (2022), https://doi.org/10.1016/j.radi.2022.03.011 no. xxxx.

[26] E.E.-D. Hemdan, M.A. Shouman, M.E. Karar, COVIDX-net: a framework of deep learning classifiers to diagnose COVID-19 in X-ray images [Online]. Available: http://arxiv.org/abs/2003.11055, 2020.

[27] J. Deng, W. Dong, R. Socher, L.-J. Li, Kai Li, Li Fei-Fei, ImageNet: A Large-Scale Hierarchical Image Database, 2010, pp. 248–255, https://doi.org/10.1109/cvpr.2009.5206848.

[28] K. Simonyan, A. Zisserman, Very Deep Convolutional Networks for Large-Scale Image Recognition, 2015.

[29] P. Huang, et al., Use of chest CT in combination with negative RT-PCR assay for the 2019 novel coronavirus but high clinical suspicion, Radiology 295 (1) (2020) 22–23, https://doi.org/10.1148/radiol.2020200330.

[30] A. Al-Bawi, K. Al-Kaabi, M. Jeryo, A. Al-Fatlawi, CCBlock: an effective use of deep learning for automatic diagnosis of COVID-19 using X-ray images, Res. Biomed. Eng. 38 (1) (2022) 49–58, https://doi.org/10.1007/s42600-020-00110-7.

[31] L. Wang, Z.Q. Lin, A. Wong, COVID-Net: a tailored deep convolutional neural network design for detection of COVID-19 cases from chest X-ray images, Sci. Rep. 10 (1) (2020), https://doi.org/10.1038/s41598-020-76550-z.

[32] C. Szegedy, S. Ioffe, V. Vanhoucke, A.A. Alemi, Inception-v4, inception-ResNet and the impact of residual connections on learning, in: 31st AAAI Conference on Artificial Intelligence, AAAI 2017, 2017, pp. 4278–4284.

[33] M. Farooq, A. Hafeez, COVID-ResNet: A Deep Learning Framework for Screening of COVID19 from Radiographs, 2020 [Online]. Available: http://arxiv.org/abs/2003.14395.

[34] H.B. Arteaga-Arteaga, et al., Deep learning applied to COVID-19 detection in X-ray images, in: Rajae El Ouazzani, et al. (Eds.), AI Applications for Disease Diagnosis and Treatment, IGI Global, 2022, pp. 202–247.

[35] S. Bekhet, M. Hassaballah, M.A. Kenk, M.A. Hameed, An artificial intelligence based technique for COVID-19 diagnosis from chest X-ray, in: 2nd IEEE Novel Intelligent and Leading Emerging Sciences Conference, 2020, pp. 191–195.

[36] S. Bekhet, M.H. Alkinani, R. Tabares-Soto, M. Hassaballah, An efficient method for covid-19 detection using light weight convolutional neural network, Comput. Mater. Continua (CMC) 69 (2) (2021) 2475–2491.

[37] A.I. Khan, J.L. Shah, M.M. Bhat, CoroNet: a deep neural network for detection and diagnosis of COVID-19 from chest x-ray images, Comput. Methods Progr. Biomed. 196 (2020), https://doi.org/10.1016/j.cmpb.2020.105581.

[38] R. Jain, M. Gupta, S. Taneja, D.J. Hemanth, Deep learning based detection and analysis of COVID-19 on chest X-ray images, Appl. Intell. 51 (3) (2021) 1690–1700, https://doi.org/10.1007/s10489-020-01902-1.

[39] I.D. Apostolopoulos, T.A. Mpesiana, Covid-19: automatic detection from X-ray images utilizing transfer learning with convolutional neural networks, Phys. Eng. Sci. Med. 43 (2) (2020) 635–640, https://doi.org/10.1007/s13246-020-00865-4.

[40] S. H. Khan et al., "COVID-19 detection in chest X-ray images using deep boosted hybrid learning," Comput. Biol. Med., vol. 137, 2021, doi: 10.1016/j.compbiomed.2021.104816.

[41] P.M. Shah, et al., Deep GRU-CNN model for COVID-19 detection from chest X-rays data, IEEE Access 10 (2022) 35094–35105, https://doi.org/10.1109/ACCESS.2021.3077592.

[42] N. Muralidharan, S. Gupta, M. R. Prusty, and R. K. Tripathy, "Detection of COVID19 from X-ray images using multiscale deep convolutional neural network," Appl. Soft Comput., vol. 119, 2022, doi: 10.1016/j.asoc.2022.108610.

[43] G. Bargshady, X. Zhou, P.D. Barua, R. Gururajan, Y. Li, U.R. Acharya, Application of CycleGAN and transfer learning techniques for automated detection of COVID-19 using X-ray images, Pattern Recogn. Lett. 153 (Jan. 2022) 67–74, https://doi.org/10.1016/j.patrec.2021.11.020.

[44] E. Luz, et al., Towards an effective and efficient deep learning model for COVID-19 patterns detection in X-ray images, Res. Biomed. Eng. 38 (1) (2022) 149–162, https://doi.org/10.1007/s42600-021-00151-6.

[45] S. Karakanis and G. Leontidis, "Lightweight deep learning models for detecting COVID-19 from chest X-ray images," Comput. Biol. Med., vol. 130, 2021, doi: 10.1016/j.compbiomed.2020.104181.

[46] Z. Gao, J. Xie, Q. Wang, P. Li, Global second-order pooling convolutional networks, in: 2019 IEEE/CVF Conference on Computer Vision and Pattern Recognition (CVPR), Jun. 2019.

[47] Y. Toda, F. Okura, How convolutional neural networks diagnose plant disease, Plant Phenomics 2019 (Mar. 2019) 1–14.

[48] P. Tania, R. Erik, C.W. Douglas, Image Statistics in Visual Computing, in: A. K. Peters (Ed.), first ed., Ltd., USA, 2013.

[49] I. Sergey, C. Szegedy, Batch normalization: accelerating deep network training by reducing internal covariate shift, in: International Conference on Machine Learning, PMLR: Lille, France, 2015, pp. 448–456.

[50] H. Dan, and K. Gimpel. Gaussian Error Linear Units (Gelus). arXiv **2016**, arXiv: 1606.08415.

[51] A. Badawi, K. Elgazzar, Detecting coronavirus from chest X-rays using transfer learning, COVID 1 (1) (Sep. 2021) 403–415, https://doi.org/10.3390/covid1010034.

[52] M.E.H. Chowdhury, T. Rahman, A. Khandakar, R. Mazhar, M.A. Kadir, Z. B. Mahbub, K.R. Islam, M.S. Khan, A. Iqbal, N.A. Emadi, M.B.I. Reaz, M.T. Islam, Can AI help in screening viral and COVID-19 pneumonia? IEEE Access 8 (2020) 132665–132676, https://doi.org/10.1109/ACCESS.2020.3010287.

[53] S.M. Pizer, R.E. Johnston, J.P. Ericksen, B.C. Yankaskas, K.E. Muller, Medical image display research group. Contrast-Limited adaptive histogram equalization: speed and effectiveness, in: Proceedings of the First Conference on Visualization in Biomedical Computing, Atlanta, GA, USA vols. 22–25, May 1990, pp. 337–345.

[54] E. Hussain, M. Hasan, M. A. Rahman, I. Lee, T. Tamanna, and M. Z. Parvez, "CoroDet: a deep learning based classification for COVID-19 detection using chest X-ray images," Chaos, Solit. Fractals, vol. 142, 2021, doi: 10.1016/j.chaos.2020.110495.

[55] S. Jadon, COVID-19 detection from scarce chest x-ray image data using few-shot deep learning approach, Med. Imaging (2021).

[56] S. Aggarwal, S. Gupta, A. Alhudhaif, D. Koundal, R. Gupta, K. Polat, Automated COVID-19 detection in chest X-ray images using fine-tuned deep learning architectures, Expet Syst. 39 (3) (Jun. 2021).

[57] V. Perumal, V. Narayanan, S.J.S. Rajasekar, Detection of COVID-19 using CXR and CT images using Transfer Learning and Haralick features, Appl. Intell. 51 (1) (August 12, 2020) 341–358, https://doi.org/10.1007/s10489-020-01831-z.

[58] D. Shome, T. Kar, S. Mohanty, P. Tiwari, K. Muhammad, A. AlTameem, Y. Zhang, A. Saudagar, COVID-transformer: interpretable COVID-19 detection using vision transformer for healthcare, Int. J. Environ. Res. Publ. Health 18 (21) (Oct. 2021) 11086, https://doi.org/10.3390/ijerph182111086.

[59] M.-L. Huang, Y.-C. Liao, A lightweight CNN-based network on COVID-19 detection using X-ray and CT images, Comput. Biol. Med. 146 (Jul. 2022) 105604.